- Dynamics and mechanisms of Mn(II), Co(II), Ni(II), Zn(II), and
- 2 Cd(II) sorption onto green rust sulfate

3

4 Khondaker M.N. Alam<sup>1</sup> and Evert J. Elzinga<sup>1\*</sup>

5

- 6 <sup>1</sup>Rutgers University
- 7 Department of Earth & Environmental Sciences
- 8 101 Warren Street
- 9 Newark, NJ 07102, U.S.A.

10

\* Corresponding author. Phone: +1 973 353 5238; Email: elzinga@newark.rutgers.edu

# **ABSTRACT**

Batch kinetic experiments were combined with X-ray absorption spectroscopy (XAS) to
compare the sorption of Mn(II), Co(II), Ni(II), Zn(II), and Cd(II) with sulfated green rust (GR) in
anoxic pre-equilibrated suspensions at pH 8 over a timespan of 1 h to 1 wk. The XAS data
suggest that all five divalent metals coordinate at Fe(II) sites of the GR sorbent, whereas the
batch results show that GR exhibits bimodal sorption behavior, with fast but limited uptake of
Mn(II) and Cd(II) and much more extensive sorption of Co(II), Ni(II), and Zn(II) that continues
throughout the entire experimental timeframe. We attribute these observations to differences in
the affinity and extent of divalent metal substitution in Fe(II) sites of the GR lattice as controlled
by ionic size. Divalent metals smaller than Fe(II) [i.e. Co(II), Ni(II), and Zn(II)] are readily
accommodated and undergo co-precipitation during GR dissolution-precipitation. In contrast,
divalent metals larger than Fe(II) [i.e. Mn(II) and Cd(II)] have a low affinity for substitution and
remain coordinated at the surface following limited exchange with $Fe(II)_{(s)}$ at GR particle edges.
These results imply that GR may strongly affect the solubility of Co(II), Ni(II), and Zn(II) in
reducing geochemical systems, but will have little impact on the retention of Cd(II) and Mn(II).
Synopsis

# 

Ionic size controls the affinity and mechanism of sorption of non redox active divalent metals by green rust: divalent metals smaller than Fe(II) undergo extensive co-precipitation, while divalent metals larger than Fe(II) remain coordinated at the surface.

Keywords

Green rust, trace metals, sorption, co-precipitation, substitution, X-ray absorption spectroscopy

#### INTRODUCTION

35

36

37

38

39

40

41

42

43

44

45

46

47

48

49

50

51

52

53

54

55

56

57

Green rust (GR) minerals are mixed-valent iron layered double hydroxides (Fe(II)-Fe(III)-LDH) that are common in natural and engineered reducing geochemical systems such as flooded soils, groundwaters, corroding drinking water lines, permeable reactive barriers, and iron electrocoagulation water treatments. 1-16 GR is a layered mineral composed of octahedral brucitic Fe(OH)<sub>2</sub> sheets in which up to 1/3 of Fe(II) has been substituted by Fe(III) to generate a positive layer charge that is balanced by interlayer anions. 1,3,17,18 Because of its high specific surface area and high content of structural ferrous Fe, GR is an effective reductant of a range of compounds including Cu(II), Hg(II), U(VI), Se(VI), and Cr(VI). 1,16,19-29 Compared to its redox reactivity, much less is known about the reactivity of GR as a sorbent of trace elements that do not undergo redox changes. We recently combined batch, XRD, and EXAFS analyses to investigate the sorption of one such redox-stable species, the trace metal Ni(II).<sup>30</sup> The work revealed that GR interacts with Ni(II) sorbates primarily through dissolutionreprecipitation reactions which lead to the incorporation of Ni(II) into the octahedral layers of Fe(II)<sub>0.67-x</sub>Ni(II)<sub>x</sub>Fe(III)<sub>0.33</sub>(OH)<sub>2</sub> LDH phases. This was notable in that Ni(II) coprecipitation occurred despite the fact that the GR sorbent was stable in the experimental suspensions, which had been pre-equilibrated before Ni(II) addition and were maintained at constant pH to avoid net GR dissolution or precipitation during sorption. Incorporation was attributed to isomorphous substitution of Ni(II) for Fe(II) during Fe(II)-driven recrystallization of the GR sorbent and/or the precipitation of mixed secondary Ni(II)/Fe(II)-Fe(III)-LDH phases with a higher stability than GR, complemented by Ni(II)<sub>(aq)</sub>-Fe(II)<sub>(s)</sub> cation exchange at GR particle edges.<sup>30</sup> The dynamic behavior of GR identified in the sorption study with Ni(II) suggests that GR may be a highly effective sink of trace metals, as co-precipitated metal sorbates are generally less soluble than mononuclear surface complexes.<sup>31,32</sup> The current study expands on this earlier work by determining the sorptive behavior of Mn(II), Co(II), Zn(II), and Cd(II), and comparing it to that of Ni(II). These are divalent metals (Me(II)) of environmental relevance that, like Ni(II), do not engage in redox reactions with GR. They exhibit differences in Me(II)-O coordination during sorption, with Zn(II) capable of forming both tetrahedral and octahedral surface complexes while the other metals favor octahedral coordination. e.g. 33-43 The five Me(II) species vary in size, with octahedral ionic radii decreasing in the order Cd(II) (0.95 Å) > Mn(II) (0.83 Å) > Co(II) (0.75 Å) ~ Zn(II) (0.745 Å) > Ni (II) (0.69 Å). <sup>44</sup> This may lead to differences in Me(II)-GR interactions, as ionic size may affect cation exchange preferences and the favorability of isomorphous Me(II) substitution into Fe(II) lattice sites in the GR bulk and at the surface. The metals further exhibit different propensities for the formation of Me(II)-Fe(III)-LDHs. Solubility products determined by Boclair and Braterman<sup>45</sup> and Bhattacharya and Elzinga<sup>46</sup> indicate that the Me(II)-Fe(III)-LDH phases formed by Co(II) and Ni(II) have similar stabilities, 45 whereas that of Zn(II)-Fe(III)-LDH is much higher, <sup>45</sup> and those of Cd(II)- and Mn(II)-Fe(III)-LDH are expected to be lower. 46 Such differences may affect the rate and extent of Me(II) coprecipitation with GR during sorption, and thereby influence the pathways of Me(II) retention.

The aim of the current study was to assess and compare the dynamics and mechanisms of the sorption of Mn(II), Co(II), Ni(II), Zn(II), and Cd(II) onto GR with combined batch experiments and spectroscopic analyses over a timespan of 1 h to 1 wk. Our results identify ionic size as a key control on the affinity and mechanisms of Me(II) sorption by GR, and provide new insights into the processes involved in trace metal retention in reducing environments.

79

58

59

60

61

62

63

64

65

66

67

68

69

70

71

72

73

74

75

76

77

## MATERIALS AND METHODS

80

81

82

83

84

85

86

87

88

89

90

91

92

93

94

95

96

97

98

99

100

101

102

**Anoxic procedures** Due to the high sensitivity of GR to oxidation by  $O_{2(g)}$ , all experimental procedures were conducted in an anaerobic glovebox using the anoxic protocols described in the Supporting Information (SI). **Synthesis of Green Rust Sulfate** Green rust with sulfate interlayer anions [Fe<sup>II</sup><sub>4</sub>Fe<sup>III</sup><sub>2</sub>(OH)<sub>12</sub>SO<sub>4</sub>·2H<sub>2</sub>O], henceforth referred to as green rust or GR, was synthesized utilizing a modified version of the co-precipitation method of Refait et al.<sup>47</sup> described in the SI. The resultant green-blue suspension (referred to as the synthesis suspension below) was aged for at least 4 d before use in the sorption experiments. **Batch Sorption Experiments** The batch sorption experiments were conducted at pH ~8.0 with pre-equilibrated GR suspensions. The suspensions were prepared by equilibrating GR solids with electrolyte set to initial pH 7.8 and amended with 0.5 mM Fe(II)SO<sub>4</sub>. Suspension pH was stabilized with 10 mM TRIS buffer (pKa = 8.06) dissolved in 0.05 M Na<sub>2</sub>SO<sub>4</sub> background electrolyte. The GR solids were harvested by vacuum filtration (0.22 µm) of 25 mL subsamples of the synthesis suspension. The solids retained on the filter paper were washed twice by filtering through two 5-mL electrolyte volumes, and then transferred to a 500 mL container. The GR solids from 10 subsamples were combined and suspended in 300 mL of electrolyte, yielding a GR suspension density of 8.2 g L<sup>-1</sup>. The container was sealed, and the suspension was aged for 2 d to equilibrate

the GR sorbent with the aqueous phase. The final pH values of the pre-equilibrated suspensions

prepared for the various experiments ranged between 7.9 and 8.1, and the dissolved Fe(II) concentrations between 0.8 and 1.5 mM.

The sorption experiments with Zn(II), Ni(II), Co(II), Mn(II), and Cd(II) were conducted with the pre-equilibrated GR suspensions described above. Two types of reactors were prepared. The first were controls consisting of pre-equilibrated GR suspensions with no added metal, while the other reactors contained pre-equilibrated GR suspensions (70 mL) that were spiked with aqueous Me(II). Spiking of the sorption reactors was done through the step-wise addition of 5 aliquots of a 0.1 M MeSO<sub>4(aq)</sub> stock solution to achieve a total Me(II) concentration of 1 mM. The suspensions were magnetically stirred during metal addition to ensure complete mixing, and pH was monitored with a double-junction pH electrode. When pH fell by 0.02 pH units, a small aliquot of 0.1 M NaOH was added for readjustment to minimize GR dissolution. Duplicate sorption and control reactors were prepared for each experiment.

Following the Me(II) spike, the concentrations of Me(II)<sub>aq</sub> and Fe(II)<sub>aq</sub> in the reactors were monitored over the course of 7 d. This was done by taking 5-mL subsamples at regular time intervals, with the first sample taken 1 h after the Me(II) spike. Each subsample was syringe-filtered through a 0.22  $\mu$ m nitrocellulose membrane into a 15-mL polyethylene tube containing 50  $\mu$ L of anoxic concentrated HCl. The acidified filtrates were analyzed for the concentrations of Me(II)<sub>aq</sub> and Fe(II)<sub>aq</sub> using ICP-OES. Suspension pH values were measured at each sampling time point as well and found to deviate by  $\leq$  0.07 pH units from the initial value in all cases. The reactors were stored in sealed ziplock bags inside the glovebox to minimize the risk of accidental oxygen intrusion. A total of 6 repeat experiments were conducted for Ni(II), 5 for Zn(II), and 2 for Co(II), Mn(II), and Cd(II).

Speciation calculations in Visual Minteq<sup>48</sup> for the initial conditions of the experiments ([Me(II)]<sub>aq</sub> = 1.0 mM; pH =8.0; I=0.05 M Na<sub>2</sub>SO<sub>4</sub>) indicated that Mn(II), Cd(II), and Co(II) were undersaturated with respect to any potential precipitate phases, while Ni(II) and Zn(II) were supersaturated with respect to  $\beta$ -Ni(OH)<sub>2</sub> and  $\beta$ -Zn(OH)<sub>2</sub>, respectively. In our previous study we demonstrated that the formation of  $\beta$ -Ni(OH)<sub>2</sub> can be ruled out in these systems.<sup>30</sup> Here we also rule out  $\beta$ -Zn(OH)<sub>2</sub> precipitation as a significant mechanism, based on the results of experiments conducted at pH 7.0 where  $\beta$ -Zn(OH)<sub>2</sub> was undersaturated showing the same Zn(II) sorption products as the main experiments (see SI section 3 and Figures S1,S2).

## X-ray Absorption Spectroscopy and X-ray Diffraction Analyses

Sorption samples for synchrotron X-ray absorption spectroscopy (XAS) were prepared for each metal with the methods described above, using sample volumes of 30 mL. The samples were reacted with Me(II)<sub>aq</sub> for 1h, 1d, or 6d, and then centrifuged to collect the GR solids. The solids were sealed into lucite sample holders with Kapton tape and transported to the synchrotron facility under anoxic conditions. The XAS data were collected at beamline 12BM of the Advanced Photon Source and beamline 6BM of the National Synchrotron Light Source II. The samples were analyzed in fluorescence mode and at room temperature at the Me *K*-edge of interest, with up to 15 scans collected per sample. Data processing and fitting was done with WinXAS3.1<sup>49</sup> in conjunction with Athena<sup>50</sup> and Feff7,<sup>51</sup> using similar procedures as in our previous study,<sup>30</sup> which are described in the SI.

Several reference compounds were prepared and analyzed for comparison with the sorption samples. These were  $Me(II)_xFe(II)_{0.67-x}Fe(III)_{0.33}(OH)_2$  LDH phases with values of x = 0.01, 0.33, and 0.67, synthesized with methods described in the SI. In the following, the

compounds with x=0.01 are referred to as Me(II):GR; those with x=0.33 as Me(II)<sub>0.5</sub>Fe(II)<sub>0.5</sub>Fe(III)-LDH; and those with x=0.67 as Me(II)-Fe(III)-LDH.

X-ray diffraction (XRD) analyses of the sorption and reference compounds were conducted to confirm phase identity and purity of the LDH phases. The analyses are described in the SI. No evidence for structural changes in the GR sorbent during the sorption experiments was observed (Figures S3, S4).

## **RESULTS AND DISCUSSION**

## **Batch Kinetic Data**

Figure 1 presents the results of the batch kinetic studies, plotting the dissolved metal levels as a function of time in the five Me(II)-GR sorption systems. Also included are the dissolved Fe(II) levels measured in the sorption and control samples. The results are the average of the multiple repeat experiments run for each metal, which are presented individually in SI Figures S5-S9. Because of the variability observed between repeat experiments (Figures S5-S9), the concentrations plotted in Figure 1 are quantified as the percentage of the initial (t=0) concentrations. The error bars of the datapoints in Figure 1 represent the standard deviation of the results from the repeat experiments. These exceed the standard deviations of the duplicate samples in individual experiments (see Figures S5-S9), and therefore mostly reflect systematic variation in the results between repeat experiments as opposed to random experimental error. The variability amounts to a maximum standard deviation of ±10% in dissolved Me(II) and Fe(II) concentrations (Figure 1), and is attributed to variations in GR sorbent properties as discussed further below.

Inspection of the sorption kinetic patterns reveals both similarities and differences between the five metals. The plots of Zn(II), Ni(II), and Co(II) display a rapid initial sorption step which removes ~32%, 35%, and 67% of aqueous Co(II), Ni(II) and Zn(II), respectively, within the first hour of reaction (Figure 1a-c). This fast initial sorption is followed by slow sorption that continues throughout the 7d timeframe of the experiments, and leads to the additional removal of 18%, 25%, and 17% of dissolved Co(II), Ni(II), and Zn(II), respectively (Figure 1a-c). These results agree with those reported previously for Ni(II), 30 and demonstrate that Co(II) has a similar affinity for GR as Ni(II) while that of Zn(II) is higher.

The kinetic plots of Mn(II) and Cd(II) notably differ from those of Co(II), Ni(II) and Zn(II) with respect to both the extent and dynamics of sorption. The uptake of aqueous Mn(II) and Cd(II) amounts to a mere 4% and 8% of initial [Mn(II)]<sub>aq</sub> and [Cd(II)]<sub>aq</sub>, respectively, and does not involve an observable stage of slow sorption (Figure 1d,e). This indicates that the tendency for sorption is much lower for Mn(II) and Cd(II) than for the other metals, and suggests that the mechanisms involved may differ.

The aqueous Fe(II) levels in the Me(II)-GR sorption samples relative to the controls provide a macroscopic indication of the response of the GR sorbent to the Me(II)<sub>aq</sub> inputs. The control samples all have stable aqueous Fe(II) concentrations (Figure 1; Figures S5-S9) confirming that they were at equilibrium throughout the experiments. Metal addition slightly perturbs the equilibrium in a manner that varies with Me(II) type (Figure 1), and to an extent that varies between repeat experiments (Figure S5-S9). Dissolved Fe(II) increases by ~20% relative to the control in the Zn(II)-GR sorption samples during the 7d reaction timeframe (Figure 1a), but by only ~4% in the Co(II)-GR systems (Figure 1c). In the Ni(II)-GR systems, in contrast, [Fe(II)]<sub>aq</sub> slightly decreases (~6%) compared to the control, while there are no changes in the

Mn(II)-GR and Cd(II)-GR systems (Figure 1b). Of note is that the changes in dissolved Fe(II) in the Ni(II), Zn(II), and Co(II) sorption experiments are much smaller than the changes in dissolved Me(II) (Figures 1a-c and S5-S7), indicating that Me(II) sorption is mostly decoupled from the release and uptake of aqueous Fe(II) in these systems.

There is variability in aqueous Fe(II) levels between repeat experiments (Figure S5-S9). This applies not only to the Fe(II)<sub>aq</sub> concentrations of the controls, which ranged between 0.8 and 1.5 mM as noted above, but also to the differences in Fe(II)<sub>aq</sub> concentration between the sorption and control samples in a given experiment. For example, the decrease in [Fe(II)]<sub>aq</sub> in the Ni(II)-GR suspensions relative to the controls ranged from negligible (Figure S5d, f) to 10% (Figure S5e), and increased Fe(II)<sub>aq</sub> levels in the Zn(II) experiments ranged from 13% to 33% (Figure S6d,e). We attribute this variability to slight variations in the properties of the GR sorbents used. Fresh GR was prepared for each experiment, and the synthesis suspensions had pH values that varied between 6.9 and 7.4 (see SI section 2). This variation in pH may have affected GR properties such as particle size and crystallinity, which are key factors determining the solubility and sorptive reactivity of GR. We argue that such differences affect the balance between the various mechanisms involved in Me(II)-GR sorption, resulting in the slight differences in outcome observed in the repeat experiments. A discussion of the mechanisms is provided below.

## **XAS Results**

The EXAFS data of the sorption and reference samples are shown in Figure 2 and Table S1, with Figure 2a presenting the raw and fitted  $k^3$ -weighted  $\chi$  functions, Figure 2b the corresponding Fourier transforms (FTs) of the raw  $\chi$  data, and Table S1 summarizing the EXAFS fit results.

The EXAFS data of the sorption samples resemble those of the reference compounds for all five metals (Figure 2), consistent with the formation of Me(II)<sub>x</sub>Fe(II)<sub>0.67-x</sub>Fe(III)<sub>0.33</sub>(OH)<sub>2</sub> LDH phases during sorption. The FTs of sorbed Me(II) display a prominent peak at  $R+\Delta R \sim 1.7$ Å (Figure 2b) representing the first-shell O neighbors of the Me(II) sorbates. The corresponding R<sub>Me(II)-O</sub> fit values are consistent with an octahedral O ligand arrangement around central Me(II), as in the Me:GR and Me-Fe(III)-LDH references (Table S1). This demonstrates that Ni(II), Zn(II), Co(II), Mn(II), and Cd(II) remain divalent during sorption and form octahedral complexes. Of the five Me(II) species, sorbed Cd(II) is the largest with  $R_{Cd-O} \sim 2.27$  Å, while sorbed Co(II), Ni(II), and Zn(II) are the smallest with  $R_{Me-O} = 2.08 \pm 0.02$  Å, and sorbed Mn(II) is intermediate with  $R_{Mn-O} \sim 2.16$  Å (Table S1). The octahedral configuration of sorbed Mn(II), Co(II), Ni(II), and Cd(II) is common and has been observed on a range of mineral sorbents. 33,34,38-43 Zn(II), on the other hand, may form both tetrahedral and octahedral sorption complexes depending on sorbent type and pH. 35-37,44,46 The two configurations can be distinguished based on the first-shell Zn-O interatomic distance, which is much shorter for tetrahedral (~1.96 Å) than for octahedral complexes (~2.08 Å). e.g.35-The values of  $R_{Zn-Q} = 2.06-2.08$  Å observed for the Zn(II)-GR sorption samples (Table S1) indicate that octahedral complexes dominate with no evidence for the substantial presence of tetrahedral Zn(II) species. The FTs of the Me(II)-GR sorption samples contain distinct second shells as well (Figure 2b). These were fitted successfully with Fe neighbors at radial distances that resemble those of the Me(II):GR references (Table S1), suggesting Me(II) substitution into the GR lattice. Structural models reported for GR with a Fe(II):Fe(III) molar ratio of 2:1 as used here 18,52-45 show that Fe(II) and Fe(III) sites have the same average Fe-Fe radial distance but differ in first-

215

216

217

218

219

220

221

222

223

224

225

226

227

228

229

230

231

232

233

234

235

236

shell Fe-O distance because of the different ionic radii of Fe(III) and Fe(II) (0.654 Å *versus* 0.78 Å <sup>44</sup>). The cation arrangement in the mineral layers is such that Fe(III) is surrounded by 6 Fe(II) neighbors, while Fe(II) is surrounded by 3 Fe(II) and 3 Fe(III) neighbors. <sup>18,52-54</sup> The avoidance of Fe(III)-Fe(III) contacts is thought to be critical to the stability of GR as it minimizes intra-lattice electrostatic repulsion, <sup>55,56</sup> and has similarly been observed for the arrangement of trivalent Al in Fe(II)-Al(III)-LDH (nikischerite) <sup>57</sup> and Mg(II)-Al(III)-LDH (hydrotalcite). <sup>58</sup> Given the importance of cation ordering to the stability of LDH phases, substitution of Me(II) is expected to occur in the Fe(II) sites of GR to maintain the arrangement of divalent and trivalent structural cations in the lattice and avoid any Fe(III)-Fe(III) clustering.

Exact identification of the coordination environment of the Me(II) sorbates is complicated by the difficulty of distinguishing between second-shell Me and Fe neighbors in  $Me(II)_xFe(II)_{0.67-x}Fe(III)_{0.33}(OH)_2$  LDH structures.<sup>30</sup> This is well illustrated by the structural similarity of the Me(II):GR and Me(II)-Fe(III)-LDH references (Table S1). In both compounds, Me(II) is in octahedral coordination with both first-shell O and second-shell Me/Fe at radial distances that differ by merely 0.02-0.04 Å (Table S1), which is at or near the estimated uncertainty of the EXAFS analyses.<sup>30</sup> The fit results of the sorption samples more closely resemble those of the Me(II):GR than the Me(II)-Fe(III)-LDH reference (Table S1). However, this only poorly constrains the coordination of the Me(II) sorbates, since fits of the Me(II)<sub>0.5</sub>-Fe(III)-LDH reference compounds are indistinguishable from those of Me(II):GR (Table S1) despite their intermediate composition between Me(II):GR and Me(II)-Fe(III)-LDH. We therefore conclude that the sorption of the five Me(II) species in our GR suspensions involves the formation of Me(II)<sub>x</sub>Fe(II)<sub>0.67-x</sub>Fe(III)<sub>0.33</sub>(OH)<sub>2</sub> LDH phases, where the value of x (0 < x  $\leq$  0.67) may span the compositional range between dilute Me(II):GR solid

solutions and pure Me(II)-Fe(III)-LDH, as proposed previously for Ni(II).<sup>30</sup> The apparent similarity in sorption mechanism of the five metals is noteworthy given the large differences in the extent and dynamics of sorption observed in the batch experiments (Figure 1), and is assessed further below.

Detailed inspection of the EXAFS data reveals several trends in the peak intensities of the second coordination shells, which are of interest because they are indicators of the structural ordering of the Me(II)/Fe(II)-Fe(III)-LDH sorption products. A first observation is that second-neighbor Fe scattering is less pronounced in the Me(II)-GR sorption samples than in the corresponding Me(II):GR and Me(II)-Fe(III)-LDH references (Figure 2b). This was noted previously for Ni(II), and likely reflects structural disorder arising from the location of Me(II) sorbates at or near the surface of GR particles rather than the bulk, and/or the physical or chemical mixing of Me(II)/Fe(II)-Fe(III)-LDH phases with variable Me(II):Fe(II) ratios.<sup>30</sup>

Secondly, the intensities of the second-shell peaks are very similar for the 1 h, 1 d and 6 d sorption samples (Figure 2b), indicating that the Me(II)/Fe(II)-Fe(III)-LDH sorption products are structurally similar regardless of reaction time. This implies that the formation of these phases does not involve slow nucleation or re-arrangement processes. Instead, they form on the same time scale as the initial fast sorption step in the batch experiments (Figure 1), and do not undergo major restructuring or ordering during subsequent ageing over 6 d.

A last noteworthy observation is that second-shell scattering in the Cd(II):GR and Mn(II):GR references and in the Cd(II) and Mn(II) sorption samples is less intense than for the other metals (Figure 2b), indicating a higher degree of disorder in the Me(II)/Fe(II)-Fe(III)-LDH phases formed by Mn(II) and Cd(II) relative to Co(II), Ni(II), and Zn(II). Mn(II) and Cd(II) are similar in that they both are larger than Fe(II), with ionic radii of 0.83 Å and 0.95 Å,

respectively, compared to 0.78 Å for Fe(II); the other three metals, in contrast, are smaller with ionic radii of 0.75 Å, 0.745 Å, and 0.69 Å for Ni(II), Zn(II), and Co(II), respectively.<sup>44</sup> Their larger sizes appear to make Mn(II) and Cd(II) a less compatible fit with the GR structure than the other metals, inducing a high degree of distortion in the lattice around the substituted sites as observed by XAS. The likely cause is the increased size mismatch with structural Fe(III), which is distinctly smaller than Fe(II) (0.645 Å versus 0.78 Å <sup>44</sup>) and appears to limit the flexibility of the GR lattice to accommodate the substitution of larger divalent impurity cations. We therefore attribute the low intensity of second-neighbor Fe scattering in the Mn(II) and Cd(II) reference and sorption samples to the relatively poor structural compatibility of these metals with the Fe(II) sites of the GR lattice. Importantly, this incompatibility translates into strongly reduced uptake of Cd(II) and Mn(II) relative to Co(II), Ni(II) and Zn(II) during GR syntheses in the presence of these metals, as observed in the preparation of the Me(II):GR reference compounds (see description in SI section 5.2 and Table S2). This indicates that Cd(II) and Mn(II) are mostly excluded from the GR lattice during co-precipitation, whereas the smaller metals are readily incorporated. This difference in affinity for isomorphous substitution as controlled by Me(II) ion size is proposed to be a major factor determining Me(II) sorption by GR, as discussed next.

300

301

302

303

304

305

306

284

285

286

287

288

289

290

291

292

293

294

295

296

297

298

299

## **Sorption Mechanisms**

The results presented here demonstrate that divalent Mn, Co, Ni, Zn, and Cd all form Me(II)/Fe(II)-Fe(III)-LDH during reaction with GR. In our previous study of Ni(II)-GR interactions,<sup>30</sup> we identified three possible pathways for the formation of these phases: (1) exchange of Me(II) cations for lattice Fe(II) exposed at GR particle edges; (2) incorporation of Me(II) into the mineral lattice during Fe(II)-catalyzed GR recrystallization; and (3) partial GR

dissolution followed by co-precipitation of Fe(II) and Fe(III) with Me(II) to form mixed Me(II)/Fe(II)-Fe(III)-LDH phases with a higher stability than GR. The current results provide new insights into the operation of these mechanisms, and suggest that their importance varies with Me(II) size and reaction time. We propose that for divalent metals larger than Fe(II) [*i.e.* Mn(II) and Cd(II)] the dominant sorption mechanism is Me(II)-Fe(II) cation exchange at GR surface sites, while for divalent metals smaller than Fe(II) [*i.e.* Co(II), Ni(II) and Zn(II)] the initial fast step of sorption (< 1 h) is dominated by coupled cation exchange and co-precipitation reactions, and slower long-term sorption (between 1d and 7d) involves Me(II) incorporation during dissolution-reprecipitation reactions of the GR sorbent.

The sorption of Mn(II) and Cd(II) stabilizes quickly (< 1 d; Figure 1d,e), and positions the metals in a structural environment similar to the Me(II):GR references as shown by the EXAFS data (Figure 2). Cation exchange with lattice Fe(II) exposed at the GR surface is consistent with these observations, since such exchange reactions equilibrate rapidly and place sorbed Me(II) into GR Fe(II) sites. The small extent of Cd(II) and Mn(II) sorption (< 8% uptake; Figure 1d,e) indicates that the exchange is not particularly favorable. This may be explained by the large ionic radii of the two metals limiting their compatibility for substitution, as noted above. A further consideration is that Me(II)-Fe(II) exchange at surface sites is subject to competition from aqueous Fe(II), which is present at a concentration equivalent to [Me(II)]<sub>aq</sub> (~1 mM; Figures S5-S9). The first hydrolysis constants of Cd(II) and Mn(II) are lower than that of Fe(II) (pK1 = 10.1, 10.6, and 9.4 for Cd(II), Mn(II), and Fe(II), respectively <sup>59</sup>). This suggests that the two metals have a lower affinity for coordination to OH surface ligands than Fe(II), <sup>60</sup> further hindering their ability to exchange for Fe(II) at GR surface sites.

The low level of uptake and lack of discernable slow sorption suggest that Cd(II) and Mn(II) do not undergo extensive incorporation into the GR lattice. The limited ability of these metals to substitute for Fe(II) at GR surface and lattice sites likely is a major factor, as this will inhibit metal incorporation during Fe(II)-catalyzed GR recrystallization. Co-precipitation is further hindered by the presumably high solubility of Cd(II)- and Mn(II)-Fe(III)-LDH relative to GR, <sup>46</sup> making the formation of mixed Me(II)/Fe(II)-Fe(III)-LDH through partial GR dissolution unlikely. We therefore conclude that Mn(II) and Cd(II) primarily sorb through fast exchange reactions with lattice Fe(II) at GR particle edges, and remain coordinated at the surface throughout the 7 d timeframe of the experiments.

The sorption of Co(II), Ni(II) and Zn(II) is much more extensive than that of Mn(II) and Cd(II), and does not reach equilibrium (Figure 1). Most Me(II)<sub>aq</sub> removal occurs during the initial (<1 h) fast step of sorption (Figure 1a-c). We argue that coupled Me(II)-Fe(II) cation exchange and co-precipitation reactions dominate this early stage of Co(II), Ni(II) and Zn(II) sorption. Key evidence are two observations: (1) the formation of well-ordered Me(II)/Fe(II)-Fe(III)-LDH phases during this time, as demonstrated by the 1-h EXAFS data (Figure 2; Table S1); and (2) the limited changes in Fe(II)<sub>aq</sub> levels during extensive initial Me(II) sorption, as observed in the batch experiments (Figure 1a-c).

Rapid Me(II)-Fe(II) exchange at the GR surface may explain the EXAFS data showing the formation of Co(II)-, Ni(II)- and Zn(II)/Fe(II)-Fe(III)-LDH within 1h of sorption (Figure 1a-c). The minor accompanying changes in dissolved Fe(II) indicate that most exchanged Fe(II) does not enter into solution but is retained by the solid phase. Although retention may involve partial re-adsorption by the GR sorbent, this mechanism cannot fully account for the lack of aqueous Fe(II) release. Elzinga<sup>30</sup> showed that the GR sorbent is capable of removing a maximum

of ~0.3 mM of any Fe(II)<sub>aq</sub> released in these systems as determined from Fe(II)-GR sorption experiments. This is distinctly lower than the concentrations of Fe(II) presumably mobilized by cation exchange with Co(II), Ni(II), and Zn(II) during the initial sorption step (0.6 – 0.8 mM; Figures 1 and S5-S7), and is likely to be lower still because of competition between Me(II) and Fe(II) for surface sites in the Me(II)-GR sorption systems. Therefore, rather than re-adsorbing, exchanged Fe(II) appears to co-precipitate with Co(II), Ni(II), and Zn(II) to form the Me(II)/Fe(II)-Fe(III)-LDH phases observed by EXAFS, in an overall process that couples Me(II)-Fe(II) exchange and co-precipitation.

352

353

354

355

356

357

358

359

360

361

362

363

364

365

366

367

368

369

370

371

372

373

374

The amounts of Co(II), Ni(II) and Zn(II) sorbed during the early reaction stages are consistent with the cation exchange and co-precipitation reactions proposed above. Sorption increases in the order Co(II) ~ Ni(II) < Zn(II) (Figure 1). This trend correlates with the first hydrolysis constants of these metals (pK1 = 9.7, 9.9, and 9.0 for Co(II), Ni(II), and Zn(II), respectively <sup>59</sup>) suggesting that Zn(II) will more readily exchange for Fe(II) at GR surface sites than Co(II) and Ni(II). The trend also correlates with the solubilities reported for the Me(II)-Fe(III)-LDH phases of the three metals. Boclair and Braterman<sup>45</sup> observed that Ni(II)- and Co(II)-Fe(III)-LDH have similar Ksp constants while that of Zn(II) is three orders of magnitude lower indicating it is much more stable. Although coprecipitation with Fe(II) likely modifies the stability of the resultant mixed Me(II)/Fe(II)-Fe(III)-LDH phases relative to pure Me(II)-Fe(III)-LDH, it is plausible that solubility differences between the three Me(II) species persist, making Zn(II)/Fe(II)-Fe(III)-LDH precipitation more favorable than Co(II)- and Ni(II)/Fe(II)-Fe(III)-LDH formation. We therefore conclude that the initial amounts of sorbed Ni(II), Zn(II), and Co(II) reflect the favorability of Me(II)/Fe(II)-Fe(III)-LDH precipitation through the coupled exchange and co-precipitation reactions dominating the early sorption stage of these metals.

At reaction times  $\geq 1$  d, ongoing sorption of Ni(II), Zn(II), and Co(II) steadily continues to remove dissolved Me(II) from solution. The levels of aqueous Fe(II) during this slow stage of sorption provide useful clues on the mechanisms at work. Distinct changes occur in the Zn(II)-GR sorption systems, where aqueous Fe(II) concentrations consistently increase relative to the control (Figure 1a, S6). Although not particularly evident in the averaged data presented in Figure 1, dissolved Fe(II) levels at reaction times > 1d generally increased concurrent with decreasing Zn(II)<sub>aq</sub> levels in the individual Zn(II)-GR sorption experiments (Figure S6), indicating that Zn(II) sorption is accompanied by partial dissolution of the GR sorbent. The slow stage of Zn(II) sorption therefore appears to involve the formation Zn(II)-LDH type phases at the expense of GR, a process that may be represented by:  $Fe^{II}_{0.67}Fe^{III}_{0.33}(OH)_{2(s)} + 0.67 Zn^{2+}_{(aq)} \rightarrow Zn^{II}_{0.67}Fe^{III}_{0.33}(OH)_{2(s)} + 0.67 Fe^{2+}_{(aq)}$ (Reaction 1) Reaction 1 involves dissolution of GR to form Zn(II)-Fe(III)-LDH, and is favorable if the Zn(II)-Fe(III)-LDH product has a higher stability than GR.<sup>30</sup> Studies directly comparing the solubilities of GR and Zn(II)-Fe(III)-LDH are not available. However, a thermodynamic study of the Al(III) variants of these phases showed that Zn(II)-Al(III)-LDH is more stable than Fe(II)-Al(III)-LDH <sup>46</sup>, and Boclair and Braterman<sup>45</sup> report that Zn(II)-Fe(III)-LDH has a very high stability with a Ksp three orders of magnitude lower than Co(II)- and Ni(II)-Fe(III)-LDH. Reaction 1 may therefore be involved in the slow stage of Zn(II) sorption, explaining the release of Fe(II) to solution. Reaction 1 defines a 1:1 stoichiometry between reactant Zn(II)<sub>aq</sub> and product Fe(II)<sub>aq</sub>. Plots of the concentrations of dissolved Zn(II) and Fe(II) in the sorption experiments show deviations from this correlation, with generally lower Fe(II)<sub>aq</sub> levels than expected (Figure S10,

375

376

377

378

379

380

381

382

383

384

385

386

387

388

389

390

391

392

393

394

395

396

397

S11). This suggests partial co-precipitation of Fe(II) with Zn(II) to form mixed Zn(II)/Fe(II)-

Fe(III)-LDH phases, similar to the early stage of sorption. Zn(II) sorption may also partially proceed through alternative pathways that do not affect [Fe(II)]<sub>aq</sub>. Of particular interest is Fe(II)-catalyzed recrystallization of the GR sorbent, which may lead to Zn(II) incorporation into the GR lattice over longer time scales. This mechanism may complement Zn(II) precipitation through reaction 1, explaining the partial decoupling of Zn(II)<sub>aq</sub> uptake from Fe(II) release during long-term sorption. However, the recrystallization of GR by aqueous Fe(II) remains to be confirmed.

Dissolution-reprecipitation of GR driven by solubility differences or coupled electronand atom-exchange reactions with Fe(II)<sub>aq</sub> may also account for the slow sorption of Ni(II) and
Co(II) (Figure 1b,c). Unlike Zn(II), however, the slow sorption of these metals occurs at steady
Fe(II)<sub>aq</sub> levels (Figures 1b,c and S5, S7). This full decoupling of Ni(II) and Co(II) uptake from
Fe(II) release indicates either that sorption is driven exclusively by Fe(II)-catalyzed
recrystallization of the GR sorbent, or that sorbate Ni(II) and Co(II) co-precipitate fully with all
Fe(II) and Fe(III) released during GR dissolution. The lack of Fe(II) release to solution implies
that the long-term Ni(II)- and Co(II)-LDH sorption products exhibit a higher degree of mixing
with Fe(II) than those of Zn(II). This may be due to the much higher stability of pure Zn(II)Fe(III)-LDH relative to Ni(II)- and Co(II)-Fe(III)-LDH, 45 making co-precipitation of Zn(II) with
Fe(II) to form mixed LDH phases less favorable than for Co(II) and Ni(II).

The coupled mechanisms of adsorption, exchange, and precipitation described above make the overall process of Me(II) sorption sensitive to changes in GR sorbent properties, in particular particle size (which controls the abundance of exchangeable Fe(II) at edge sites <sup>30,62</sup>) and crystallinity (which determines the solubility and stability of the GR sorbent). The variations observed between repeat experiments likely are due to such differences in sorbent GR

properties, as noted above. For example, the variation in [Zn(II)]<sub>aq</sub>:[Fe(II)]<sub>aq</sub> stoichiometries during long-term sorption in the repeat Zn(II)-GR sorption experiments (Figures S6 and S11) may reflect differences in GR solubility that shift the relative importance of slow Zn(II) sorption through Fe(II)-catalyzed recyrstallization *versus* solubility-driven GR dissolution-reprecipitation. Similarly, differences in GR particle size may affect Me(II) surface coverage and thereby the impact of Me(II) sorption on GR solubility. This and possibly other factors may account for the variations observed in the Ni(II) sorption systems, where in some experiments addition of Ni(II) slightly lowers [Fe(II)]<sub>aq</sub> (by <10%) while in other experiments [Fe(II)]<sub>aq</sub> is unaffected (Figure S5). Resolving these observational details will require further study of the prevailing sorption mechanisms and the ways they interact.

## **ENVIRONMENTAL IMPLICATIONS**

The results of this study show that GR displays bimodal behavior as a sorbent of the five Me(II) species studied here: the divalent metals smaller than Fe(II) [i.e. Co(II), Ni(II) and Zn(II)] are sorbed extensively and continue to be removed from solution over extended time scales, while the divalent metals larger than Fe(II) [Mn(II) and Cd(II)] are sorbed rapidly but only in limited amounts. We deduce that these sorption behaviors reflect different sorption modes, where the smaller divalent metals undergo co-precipitation that lead to structural incorporation into the GR lattice, while the larger divalent metals remain coordinated at the surface. These metal-specific differences in sorption capacity and mechanisms imply that GR will have little impact on the retention of Cd(II) and Mn(II) in reducing environments, but may strongly affect the solubility of Co(II), Ni(II), and Zn(II).

The co-precipitation and substitution processes identified here as the dominant mechanisms of Me(II) sorption onto GR will affect the structure and composition of the near-surface GR mineral lattice, and as a result may impact GR stability and reactivity. This is consistent with the results of recent studies showing that sorbed metals [including Ni(II), Mn(II) and Zn(II)] accelerate the mineralogical conversion of GR to Fe(III)-oxides during exposure to oxygen <sup>63,64</sup> and heating, <sup>65</sup> and may promote the reductive dechlorination of chlorinated hydrocarbons by GR. <sup>66</sup> The observed effects are metal-specific, <sup>63,65,66</sup> which is likely due at least in part to the differences in sorption behavior identified here. As an example, Wang et al. <sup>63</sup> report that Ni(II) sorbates more strongly promote the oxidative transformation of GR by O<sub>2(g)</sub> than Mn(II), consistent with the more extensive association of Ni(II) with GR observed in the current experiments. Additional characterization of the impacts of Me(II) sorbates on GR reactivity and of the underlying mechanisms is important for understanding the behavior of naturally occurring GR, which may contain appreciable levels of metal impurities. <sup>9,63,67,68</sup>

The stability of GR and other LDH phases is affected by the identity of the interlayer anions that neutralize the layer charge. 1,69,70 Currently available thermodynamic data indicate that GR-carbonate is more stable than GR-sulfate. 1,69,71,72 Since our results suggest that GR solubility plays an important role in controlling the mechanisms of Me(II) sorption, the sorptive behavior of GR may be quite different in freshwater environments dominated by GR-carbonate 5 than in saline systems dominated by GR-sulfate. 73 Systematic studies of the impacts of the interlayer counteranions on GR sorption behavior are needed to assess this further.

The control of ionic size identified here for the sorption of Mn(II), Co(II), Ni(II), Zn(II) and Cd(II) sorption by GR may apply to other geochemically relevant divalent cations as well, including Mg(II) and Cu(II) [both smaller than Fe(II)], and Pb(II) and Hg(II) [both larger than

Fe(II)]. However, factors other than ionic size, particularly redox changes [as observed for Cu(II) and Hg(II)<sup>74,75</sup>] and deviations from octahedral coordination during sorption [common for Pb(II) and Cu(II) <sup>e.g. 76-80</sup>] must also be considered, as these may modulate or override the effects of size alone. The delineation of these various controls on the sorptive reactivity of Me(II) species with GR will require further experimental work.

#### **ACKNOWLEDGMENTS**

This reseach was supported by the U.S. National Science Foundation through grant CHE-1904981. The authors acknowledge Argonne National Laboratory for use of Beamline 12BM at the Advanced Photon Source, a US Department of Energy Office of Science User Facility operated for the DOE office of Science by Argonne National Laboratory under contract DE-AC02-06CH11357. The work also used beamline 6BM of the National Synchrotron Light Source II, a US Department of Energy Office of Science User Facility operated for the DOE Office of Science by Brookhaven National Laboratory under Contract No. DE-SC0012704. We thank Sungsik Lee and Benjamin Reinhart (APS 12BM) and Bruce Ravel (NSLS-II 6BM) for assistance with XAS data collection. We further thank Associate Editor Daniel Giammar and two anonymous reviewers for their helpful comments that improved this paper.

# SUPPORTING INFORMATION AVAILABLE

(1) Description of the anoxic protocols used for the experiments; (2) Description of the GR synthesis procedure; (3) XAS and batch sorption results of Zn(II)-GR samples prepared under initial conditions undersaturated with respect to  $\beta$ -Zn(OH)<sub>2(s)</sub>; (4) Description of EXAFS data fitting procedures; (5) Table with EXAFS fit results; (6) Description of the methods used for

- 489 synthesizing the Me(II)<sub>x</sub>Fe(II)<sub>0.67-x</sub>Fe(III)<sub>0.33</sub>(OH)<sub>2</sub> LDH reference compounds; (7) XRD
- 490 analyses results of the sorption and reference samples; (8) Batch kinetic sorption results of the
- 491 individual Me(II)-GR repeat experiments.

492

493

#### REFERENCES

494 (1) Usman, M.; Byrne, J.M.; Chaudhary, A.; Orsetti, S.; Hanna, K.; Ruby, C.; Kappler, A.; 495 Haderlein, S.B. Magnetite and green rust: Synthesis, properties, and environmental 496 applications of mixed-valent iron minerals. Chem. Reviews 2018, 118, 3251-3304.

497

498 (2) Trolard, F.; Genin, J.M.R.; Abdelmoula, M.; Bourrie, G.; Humbert, B.; Herbillon, A. 499 Identification of a green rust mineral in a reductomorphic soil by Mossbauer and Raman 500 spectroscopies. Geochim. Cosmochim. Acta 1997, 61, 1107-1111.

501

502 Trolard, F.; Bourri G. Geochemistry of Green Rusts and Fougerite: A Reevaluation of (3) 503 Fe cycle in Soils. Advances in Agronomy 2008, 99, 227–288.

504

505 Genin, J.M.R.; Bourrie, G.; Herbillon, A.; Abdelmoula, M.; Jaffrezic, A.; Refait, P.; **(4)** 506 Maitre, V.; Humbert, B.; Herbillon, A. Thermodynamic equilibria in aqueous suspensions 507 of synthetic and natural Fe(II)-Fe(III) green rusts: Occurrences of the mineral in 508 hydromorphic soils. Environ. Sci. Technol. 1998, 32, 1058-1068.

509

510 Christiansen, B. C.; Balic-Zunic, T.; Dideriksen, K.; Stipp, S. L. S. Identification of (5) 511 Green Rust in Groundwater. Environ. Sci. Technol. 2009, 43, 3436-3441.

512

513 Bearcock, J.; Perkins, W.; Dinelli, E.; Wade, S. Fe(II)/Fe(III) 'Green Rust' Developed (6) 514 within Ochreous Coal Mine Drainage Sediment in South Wales, UK. Min. Magazine 515 **2006**, 70, 731–741.

516

517 Zegeye, A.; Bonneville, S.; Benning, L.G.; Sturm, A.; Fowle, D.A.; Jones, C.; Canfield, **(7)** 518 D.E.; Ruby, C.; MacLean, L.C.; Nomosatryo, S.; Crowe, S.A.; Poulton, S.W. Green rust 519 formation controls nutrient availability in a ferruginous water column. Geology 2012, 40, 520 599-602.

521

522 (8) Root, R.A.; Dixit, S.; Campbell, K.M.; Jew, A.D.; Hering, J.G.; O'Day, P.A. Arsenic 523 sequestration by sorption processes in high-iron sediments. Geochim. Cosmochim. Acta 524 **2007**, 71, 5782–5803.

525

526 (9) Johnson, C.A.; Freyer, G.; Fabisch, M.; Caraballo, M.A.; K sel, K.; Hochella, M.F. 527 Observations and Assessment of Iron Oxide and Green Rust Nanoparticles in Metal-528 Polluted Mine Drainage within a Steep Redox Gradient. Environ. Chem. 2014, 11,

377-391. 529

530
 531 (10) Rennert, T.; Eusterhues, K.; De Andrade, V.; Totsche, K.U. Iron Species in Soils on a
 532 Mofette Site Studied by Fe K-Edge X-Ray Absorption near-Edge Spectroscopy. *Chem.* 533 *Geology* 2012, 332/333, 116–123.

534

Weatherington-Rice, J.; Bigham, J. M. Buried Pre-Illinoian-Age Lacustrine Deposits with "Green Rust" Colors in Clermont County, Ohio. *Ohio J. Sci.* **2006**, *106*, 35–44.

537

538 (12) Swietlik, J.; Raczyk-Stanislawiak, U.; Piszora, P.; Nawrocki, J. Corrosion in drinking water pipes: The importance of green rusts. *Water Research* **2012**, *46*, 1-10.

540

541 (13) Roh, Y.; Lee, S.Y.; Elless, M.P. Characterization of corrosion products in the permeable reactive barriers. *Environ. Geology* **2000**, *40*, 184-194.

543

544 (14) Dubrawski, K.L.; van Genuchten, C.M.; Delaire, C.; Amrose, S.E.; Gadgil, A.J.; 545 Mohseni, M. Production and transformation of mixed-valent nanoparticles generated by 546 Fe(0) electrocoagulation. *Environ. Sci. Technol.* **2015**, *49*, 2171-2179.

547

Van Genuchten, C.M.; Behrends, T.; Kraal, P.; Stipp, S.L.S.; Dideriksen, K. Controls on the formation of Fe(II,III) (hydr)oxides by Fe(0) electrolysis. *Electrochim. Acta* **2018**, 286, 325-3381.

551

552 (16) Bae, Y.; Crompton, N.M.; Sharma, N.; Yuan, Y.; Catalano, J.G.; Giammar, D.E. Impact of dissolved oxygen and pH on the removal of selenium from water by iron electrocoagulation. *Water Res.* **2022**, *213*, 118159.

555

556 (17) Hansen, H.C.B. 2001. Environmental Chemistry of Iron(II)-Iron(III) LDHs (Green Rusts). In: Layered Double Hydroxides: Present and Future; Nova Science Publishers, Huntington, NY, p. 469–493.

559

Christiansen, B. C.; Balic-Zunic, T.; Petit, P. O.; Frandsen, C.; Mørup, S.; Geckeis, H.;
 Katerinopoulou, A.; Stipp, S. L. S. Composition and structure of an iron-bearing, layered double hydroxide (LDH) – Green rust sodium sulphate. *Geochim. Cosmochim. Acta* 2009, 73, 3579-3592.

564

565 (19) Legrand, L.; El Figuigui, A.; Mercier, F.; Chausse, A. Reduction of aqueous chromate by Fe(II)/Fe(III) carbonate green rust: Kinetic and mechanistic studies. *Environ. Sci.*567 *Technol.* **2004**, 38, 4587–4595.

568

Williams A. G. B.; Scherer M. M. Kinetics of Cr(VI) reduction by carbonate green rust.
 *Environ. Sci. Technol.* 2001, 35, 3488–3494.

571

572 (21) Bond, D. L.; Fendorf, S. Kinetics and Structural Constraints of Chromate Reduction by Green Rusts. *Environ. Sci. Technol.* **2004**, *37*, 2750–2757.

- Loyaux-Lawniczak, S.; Refait, P.; Ehrhardt, J. J.; Lecomte, P.; G nin, J. M. R. Trapping of Cr by Formation of Ferrihydrite During the Reduction of Chromate Ions by Fe(II)-Fe(III) Hydroxysalt Green Rusts. *Environ. Sci. Technol.* **2000**, 34, 438–443.
- 579 (23) Latta, D.; Boyanov, M.; Kemner, K.; O'Loughlin, E.; Scherer, M. Reaction of
  580 Uranium(VI) with Green Rusts: Effect of Interlayer Anion. *Current Inorg. Chem.* **2015**,
  581 5, 156–168.

578

589

600

604

607

610

- O'Loughlin, E. J.; Kelly, S. D.; Kemner, K. M.; Csencsits, R.; Cook, R. E. Reduction of Ag<sup>I</sup>, Au<sup>III</sup>, Cu<sup>II</sup>, and Hg<sup>II</sup> by Fe<sup>II</sup>/Fe<sup>III</sup> Hydroxysulfate Green Rust. *Chemosphere* **2003**, *53*, 437–446.
- 587 (25) Myneni, S. C. B.; Tokunaga, T. K.; Brown, G. E. Abiotic selenium redox transformations in the presence of Fe(II,III) Oxides. *Science* **1997**, *278*, 1106–1109.
- 590 (26) Lee, W.; Batchelor, B. Reductive Capacity of Natural Reductants. *Environ. Sci. Technol.* 591 **2003**, *37*, 535–541.
- 593 (27) Skovbjerg, L.L.; Stipp, S.L.S.; Utsunomiya, S.; Ewing, R. C. The Mechanisms of 594 Reduction of Hexavalent Chromium by Green Rust Sodium Sulphate: Formation of Cr-595 Goethite. *Geochim. Cosmochim. Acta* **2006**, *70*, 3582–3592.
- 597 (28) O'Loughlin, E. J.; Kelly, S. D.; Kemner, K. M. XAFS investigation of the interactions of U(VI) with secondary mineralization products from the bioreduction of Fe(III) oxides.
  599 Environ. Sci. Technol. 2010, 44, 1656-1661.
- 601 (29) O'Loughlin, E. J.; Kelly, S. D.; Cook, R. E.; Csencsits, R.; Kemner, K. M. Reduction of uranium(VI) by mixed iron(II)/iron(III) hydroxide (green rust): Formation of UO<sub>2</sub> 603 nanoparticles. *Environ. Sci. Technol.* **2003**, *37*, 721-727.
- 605 (30) Elzinga, E.J. Mechanistic study of Ni(II) sorption by green rust sulfate. *Environ. Sci. Technol.* **2021**, 55, 10411-10421.
- 608 (31) Sparks, D.L. **2002**. Environmental Soil Chemistry. Academic Press, San Diego, California.
- Reeder, R.J.; Schoonen, M.A.A.; Lanzirotti, A. Metal Speciation and its role in bioaccessibility and bioavailability. *Rev. Mineral. Geochem.* **2006**, *64*, 59-113.
- 614 (33) Bochatay, L.; Persson, P.; Sjoberg, S. Metal ion coordination at the water-manganite (γ-615 MnOOH) interface: An EXAFS study of cadmium(II). *J. Colloid Interf. Sci*, **2000**, *229*, 616 584-592.
- Van Groeningen, N.; Gluck, B.; Christl, I.; Kretzschmar, R. Surface precipitation of Mn<sup>2+</sup> on clay minerals enhances Cd<sup>2+</sup> sorption under anoxic conditions. *Environ. Sci. Processes Impacts*, **2020**, *22*, 1654-1665.

Waychunas, G.A.; Fuller, C.C.; Davis, J.A. Surface complexation and precipitate geometry for aqueous Zn(II) sorption on ferrihydrite I: X-ray absorption extended fine structure spectroscopy and analysis. *Geochim. Cosmochim. Acta* **2002**, *66*, 1119-1137.

621

633

645

652

656

663

626 (36) Roberts, D.R.; Ford, R.G.; Sparks, D.L. Kinetics and mechanisms of Zn complexation on metal oxides using EXAFS spectroscopy. *J. Colloid Interf. Sci.* **2003**, *263*, 364-376.

- 629 (37) Elzinga, E.J.; Reeder, R.J. . X-ray absorption spectroscopy study of Cu<sup>2+</sup> and Zn<sup>2+</sup>
  630 adsorption complexes at the calcite surface: Implications for site-specific metal
  631 incorporation preferences during calcite crystal growth. *Geochim. Cosmochim. Acta*632 **2001**, 66, 3943-3954.
- (38) Farquhar, M.L.; Vaughan, D.J.; Hughes, C.R.; Charnock, J.M.; England, K.E.R.
   Experimental studies of the interaction of aqueous metal cations with mineral substrates:
   Lead, cadmium, and copper with perthitic feldspar, muscovite, and biotite. *Geochim.* Cosmochim. Acta 1997, 61, 3051-3064.
- 639 (39) Namgung, S.; Guo, B.; Sasaki, K.; Lee, S.S.; Lee, G. Macroscopic and microscopic behaviors of Mn(II) (ad)sorption to goethite with the effects of dissolved carbonates under anoxic conditions. *Geochim. Cosmochim.Acta* **2020**, *277*, 300-319.
- 643 (40) Arai, Y. Spectroscopic evidence for Ni(II) surface speciation at the iron oxyhydroxide-644 water interface. *Environ. Sci. Technol.* **2008**, *42*, 1151-1156.
- 646 (41) Flynn, E.D.; Catalano, J.G. Competitive and cooperative effects during nickel adsorption 647 to iron oxides in the presence of oxalate. *Environ. Sci. Technol.* **2017**, *51*, 9792-9799.
- 649 (42) Chen, C.C.; Hayes, K.F. X-ray absorption spectroscopy investigation of aqueous Co(II) 650 and Sr(II) sorption at clay-water interfaces. *Geochim. Cosmochim. Acta*, **1999**, *63*, 3205-651 3215.
- 653 (43) O'Day, P.A.; Parks, G.A.; Brown, G.E. Molecular structure and binding sites of cobalt(II) surface complexes on kaolinite from X-ray absorption spectroscopy. *Clays Clay Miner.* **1994**, *42*, 337-355.
- 657 (44) Shannon, R.D. Revised effective ionic radii and systematic studies of interatomic distances in halides and chalcogenides. *Acta Cryst.* **1976**, *A32*, 751-767.
- 660 (45) Boclair, J.W.; Braterman, P.S. Layered double hydroxides. 1. Relative stabilities of layered double hydroxides and their simple counterparts. *Chem. Mater.* **1999**, *11*, 298-302.
- 664 (46) Bhattacharya L.; Elzinga E.J. A comparison of the solubility products of layered Me(II)665 Al(III)-hydroxides based on sorption studies with Ni(II), Zn(II), Co(II), Fe(II) and Mn(II).
  666 Soil Systems 2018, 2, 20. DOI: 10.3390/soilsystems2020020.

668 (47) Refait, P.; G hin, A.; Abdelmoula, M.; G nin, J.M.R. Coprecipitation Thermodynamics of iron(II-III) Hydroxysulphate Green Rust from Fe(II) and Fe(III) Salts. *Corrosion Sci.*670 **2003**, 45, 659–676.

671

667

672 (48) Gustaffson, J.P. Visual MINTEQ chemical equilibrium model version 3.1. Stockholm 673 Royal Institute of Technology (KTH), Stockholm, Sweden, 2017.

674

675 (49) Ressler, T. WinXAS: A new software package not only for the analysis of energydispersive XAS Data. *J. Phys. IV France* **1997**, *7*, C2-269

677

678 (50) Ravel, B.; Newville, M. ATHENA, ARTEMIS, HEPHAESTUS: data analysis for X-ray absorption spectroscopy using IFEFFIT. *J. Synchrotron Radiat.* **2005**, *12*, 537-541.

680

681 (51) Ankudinov, A. L.; Rehr, J. J. Relativistic calculations of spin-dependent X-ray absorption spectra. *Phys. Rev. B* **1997**, *56*, R1712-R1715.

683

684 (52) Simon, L.; Francois, M.; Refait, P.; Renaudin, G.; Lelaurain, M.; Genin, J.M.R. Structure 685 of the Fe(II-III) layered double hydroxysulphate green rust two from Rietveld analysis. 686 *Solid State Sci.* **2003**, *5*, 327–334.

687

688 (53) Aissa, R.; Francois, M.; Ruby, C.; Fauth, F.; Medjahdi, G.; Abdelmoula, M.; G nin, J. M. Formation and crystallographical structure of hydroxysulphate and hydroxycarbonate green rusts synthetised by coprecipitation. *J. Phys. Chem. Solids* **2006**, *67*, 1016–1019.

691

692 (54) Refait, P. H.; Abdelmoula, M.; G nin, J. M. R. Mechanisms of formation and structure of green rust one in aqueous corrosion of iron in the presence of chloride ions. *Corros. Sci.* **1998**, *40*, 1547–1560.

695

696 (55) Trolard, F.; Bourrié, G. Geochemistry of Green Rusts and Fougerite: A Reevaluation of Fe cycle in Soils. *Adv. Agron.* **2008**, *99*, 227–288.

698

(56) Refait, P.; Abdelmoula, M.; Trolard, F.; Génin, J.M.R.; Ehrhardt, J.J.; Bourrié, G.
 Mössbauer and XAS study of green rust mineral; the partial substitution of Fe<sup>2+</sup> by Mg<sup>2+</sup>.
 Am. Mineralog. 2001, 86, 731-739

702

703 (57) Huminicki, D.M.C.; Hawthorne, F.C. The crystal structure of nikischerite,
704 NaFe<sup>2+</sup>6Al<sub>3</sub>(SO<sub>4</sub>)<sub>2</sub>(OH)<sub>18</sub>(H<sub>2</sub>O)<sub>12</sub>, a mineral of the shigaite group. *Can. Mineral.* **2003**, 41,
705 79-82.

706

707 (58) Sideris, P.; Nielsen, U.O.; Gan, Z.; Grey, C.P. Mg/Al ordering in layered double 708 hydroxides revealed by multinuclear NMR spectroscopy. *Sci.* **2008**, *321*, 113-117.

709

710 (59) Smith, R.M.; Martell, A.E. NIST Standard Reference Database 46: NIST Critically
 711 Selected Stability Constants of Metal Complexes Database. National Institute of Standards
 712 and Technology, Gaithersburg, Maryland, 2004.

713
714 (60) Kinniburgh, D.G.; Jackson, M.L.; Syers, J.K. Adsorption of alkaline earth, transition, and heavy metal cations by hydrous oxide gels of iron and aluminum. *Soil Sci. Soc. Am. J.*716 **1976**, *40*, 796-799.

717

718 (61) Gorski C.A.; Fantle M.S. Stable mineral recrystallization in low temperature aqueous systems: A critical review. *Geochim. Cosmochim. Acta* **2017**, *198*, 439-465.

720

721 (62) Dideriksen, K.; Voigt, L.; Mangayayam, M.C.; Eiby, S.H.; van Genuchten, C.M.; 722 Frandsen, C.; Jensen, K.M.Ø.; Stipp, S.L.S.; Tobler, D.J. Order and Disorder in Layered 723 Double Hydroxides: Lessons Learned from the Green Rust Sulfate -Nikischerite Series. 724 ACS Earth Space Chem. 2022, 6, 2, 322–332

725

726 (63) Wang, X.; Peng, J.; Liang, X.; Zhu, M.; Lanson, B.; Wang, L.; Liang, X.; Liu, F.; Tan, W.; Feng. X. Effects of Mn<sup>2+</sup>, Ni<sup>2+</sup>, and Cu<sup>2+</sup> on the Formation and Transformation of Hydrosulfate Green Rust: Reaction Processes and Underlying Mechanisms. *ACS Earth Space Chem.* **2019**, *3*, 519–530.

730

731 (64) Inoue, K.; Kwon, S. K.; Kimijima, K.; Kanie, K.; Muramatsu, A.; Shinoda, K.; Suzuki, S.; Waseda, Y. Analysis of iron oxyhydroxides and oxides converted from green rust in aqueous solution. *ISIJ Int.* **2007**, *47*, 453–457.

734

735 (65) Farr, O.; Elzinga, E.J.; Yee, N. Effect of Ni<sup>2+</sup>, Zn<sup>2+</sup>, and Co<sup>2+</sup> on green rust transformation to magnetite. *Geochem. Trans.* **2022**, *23*, 3.

737

738 (66) O'Loughlin, E.J.; Boyanov, M.I.; Kemner, K.M.; Burris, D.R. Effects of Metal
 739 Amendments on the Reductive Dechlorination of Carbon Tetrachloride by Green Rust.
 740 ChemRxiv. Cambridge: Cambridge Open Engage 2022, DOI: 10.26434/chemrxiv-2022-zsx7m.

742

743 (67) Johnson, C. A.; Murayama, M.; Kusel, K.; Hochella, M. F. Polycrystallinity of green rust 744 minerals and their synthetic analogs: Implications for particle formation and reactivity in 745 complex systems. *Am. Mineral.* **2015**, *100*, 2091–2105.

746

747 (68) Genin, J. M. R.; Aissa, R.; Gehin, A.; Abdelmoula, M.; Benali, O.; Ernstsen, V.; Ona-748 Nguema, G.; Upadhyay, C.; Ruby, C. Fougerite and Fe<sup>II-III</sup> hydroxycarbonate green rust; 749 ordering, deprotonation and/or cation substitution; structure of hydrotalcite-like 750 compounds and mythic ferrosic hydroxide Fe(OH)<sub>(2+x)</sub>. *Solid State Sci.* **2005**, *7*, 545–572.

751

752 (69) Bourdoiseau, J. A.; Sabot, R.; Jeannin, M.; Termemil, F.; Refait, P. Determination of Standard Gibbs Free Energy of Formation of Green Rusts and Its Application to the Fe(II–III) Hydroxy-Oxalate. *Colloids Surf.*, A **2012**, 410, 72–80.

755

756 (70) Peltier, E.; Allada, R.; Navrotsky, A.; Sparks, D.L. Nickel solubility and precipitation in soils: a thermodynamic study. *Clays Clay Miner.* **2006**, *54*, 153–164.

759 (71) Refait, P.; Bon, C.; Simon, L.; Bourri, G.; Trolard, F.; Bessiere, J.; G nin, J.-M.
 760 Chemical composition and Gibbs standard free energy of formation of Fe(II)-Fe(III)
 761 hydroxysulphate green rust and Fe(II) Hydroxide. Clay Miner. 1999, 34, 499-510.

762

773

777

786

790

- 763 (72) Ayala-Luis, K. B.; Koch, C. B.; Hansen, H. C. B. The standard Gibbs energy of formation of Fe(II)Fe(III) hydroxide sulfate green rust. *Clays Clay Miner*. **2008**, *56*, 633–644.
- (73) Genin, J. M. R.; Olowe, A. A.; Benbouzid-Rollet, N.D.; Prieur, D.; Confente, M.; Resiak,
   B. The simultaneous presence of green rust 2 and sulfate reducing bacteria in the corrosion of steel sheet piles in a harbour area. *Hyperfine Interact.* 1992, 69, 875–878.
- 770 (74) O'Loughlin, E.J.; Kelly, S.D.; Kemner, K.M.; Csencsits, R.; Cook, R.E. Reduction of 771 Ag(I), Au(III), Cu(II), and Hg(II) by Fe(II)/Fe(III) hydroxysulfate green rust. 772 *Chemosphere* **2003**, *53*, 437-46.
- 774 (75) Maithreepala, R.A.; Doong, R. Enhanced Dechlorination of Chlorinated Methanes and 775 Ethenes by Chloride Green Rust in the Presence of Copper(II). *Environ. Sci.* 776 *Technol.* **2005**, *39*, 4082–4090.
- (76) Elzinga, E.J.; Rouff, A.A.; Reeder, R.J. The long-term fate of Zn<sup>2+</sup>, Cu<sup>2+</sup> and Pb<sup>2+</sup>
   adsorption complexes at the calcite surface: An X-ray absorption spectroscopy study.
   *Geochim. Cosmochim. Acta*, 2006,70, 2715-2725.
- 782 (77) Bargar, J.R.; Brown, G.E.; Parks, G.A. Surface complexation of Pb(II) at oxide-water 783 interfaces: II. XAFS and bond-valence determination of mononuclear Pb(II) sorption 784 products and surface functional groups on iron oxides. *Geochim. Cosmochim. Acta* **1997**, 785 61, 2639-2652.
- 787 (78) Strawn, D.G.; Scheidegger, A.M.; Sparks, D.L. Kinetics and Mechanisms of Pb(II)
  788 Sorption and Desorption at the Aluminum Oxide–Water Interface. *Environ. Sci.*789 *Technol.* **1998**, *32*, 17, 2596–2601
- 791 (79) Alcacio, T,E,; Hesterberg, D.; Chou, J.W.; Martin, J.D.; Beauchemin, S.; Sayers, D.E.
   792 Molecular scale characteristics of Cu(II) bonding in goethite-humate complexes. *Geochim. Cosmochim. Acta* 2001, 65, 1355-1366.
- 795 (80) Chesne, R.B.; Kim, C.S. Zn(II) and Cu(II) adsorption and retention onto iron 796 oxyhydroxide nanoparticles: effects of particle aggregation and salinity. *Geochem Trans*. 797 **2014**, *15*, 6.

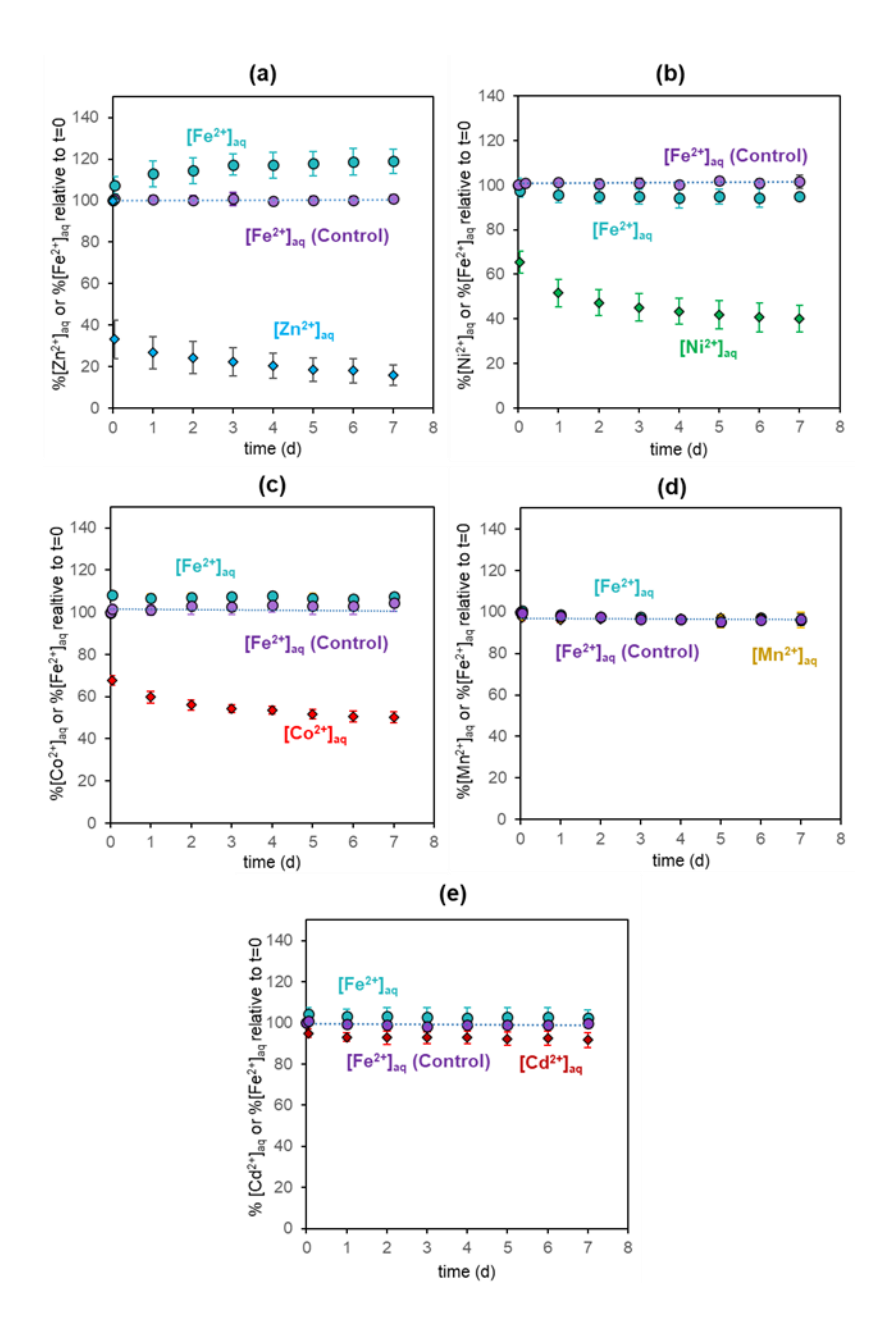


**Figure 1**. Results of the batch kinetic sorption studies conducted with (a) Zn(II), (b) Ni(II), (c) Co(II), (d) Mn(II) and (e) Cd(II) and the corresponding controls without added Me(II). The data points represent the dissolved Me(II) and Fe(II) concentrations quantified as the percentage of the initial (t=0) concentration. The experiments were run at  $pH \sim 8$  using anoxic GR suspensions with a density of 8.2 g  $L^{-1}$ , a background electrolyte of 0.05 M  $Na_2SO_4$  and 10 mM Tris, and an initial aqueous Me(II) concentration of  $\sim 1.0$  mM. The diamond data markers represent the dissolved Me(II) concentrations and the round markers the dissolved Fe(II) levels in the sorption samples and controls. The data are the average of five and six repeat experiments respectively for Zn(II) and Ni(II), and of two repeat experiments each for Co(II), Mn(II) and Cd(II); the error bars symbolize the corresponding standard deviations. The individual experiments are presented in SI Figures S5-S9.

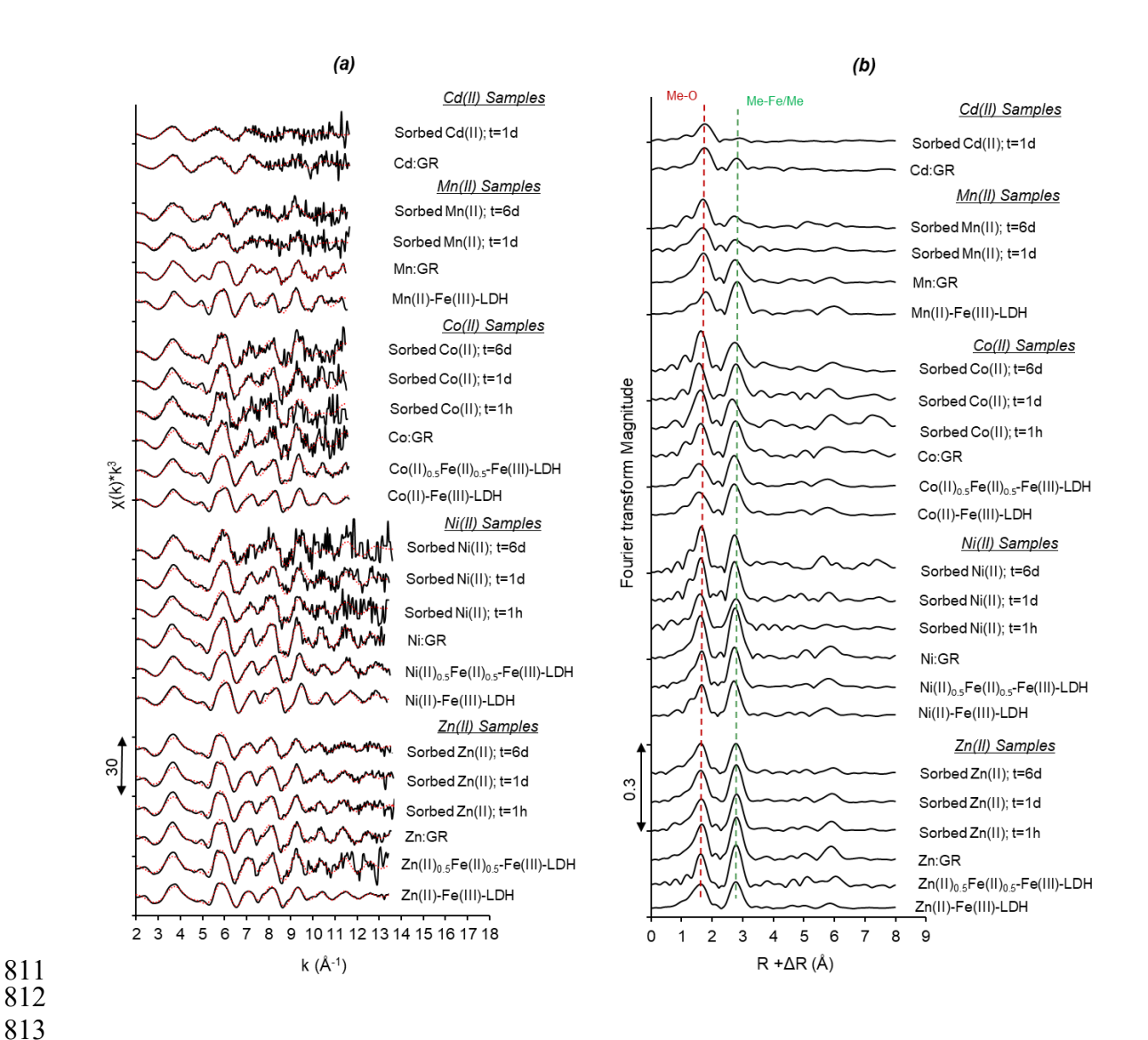


Figure 2. Me K-edge EXAFS data of the sorption samples and reference compounds: (a) k<sup>3</sup>weighted raw (black lines) and fitted (red lines) χ spectra; (b) corresponding Fourier transforms (FTs) of the raw spectra (uncorrected for phase shift). The scaling of the y-axes is indicated by the double-arrow scale bars. The vertical dotted lines in panel (b) locate the first-shell O and second-shell Fe/Me atomic neighbors surrounding sorbed Me(II). The fit results are summarized in SI Table S1.

822 TOC art

